

Extragalactic Proper Motions: Gravitational Waves and Cosmology

Jeremy Darling¹, Alexandra Truebenbach¹, and Jennie Paine¹

¹*Center for Astrophysics and Space Astronomy, Department of Astrophysical and Planetary Sciences, University of Colorado, 389 UCB, Boulder, CO 80309-0389, USA*

Abstract. Extragalactic proper motions can reveal a variety of cosmological and local phenomena over a range of angular scales. These include observer-induced proper motions, such as the secular aberration drift caused by the solar acceleration about the Galactic Center and a secular extragalactic parallax resulting from our motion with respect to the cosmic microwave background rest frame. Cosmological effects include anisotropic expansion, transverse peculiar velocities induced by large scale structure, and the real-time evolution of the baryon acoustic oscillation. Long-period gravitational waves can deflect light rays, producing an apparent quadrupolar proper motion signal. We review these effects, their imprints on global correlated extragalactic proper motions, their expected amplitudes, the current best measurements (if any), and predictions for *Gaia*. Finally, we describe a possible long-baseline ngVLA program to measure or constrain these proper motion signals. In most cases, the ngVLA can surpass or complement the expected end-of-mission performance of the *Gaia* mission.

1. Background

The universe is dynamic, as we know from cosmological redshifts induced by the Hubble expansion, but astronomers tend to treat extragalactic objects as fixed in the sky with fixed apparent velocities. If measured with enough precision, however, nothing is constant: all objects will change their redshifts and positions at a rate of order $H_0 \approx 7 \times 10^{-11} \text{ yr}^{-1} \approx 15 \mu\text{arcsec yr}^{-1}$. The secular redshift drift caused by a non-constant expansion (Sandage 1962) is of order $0.3 \text{ cm s}^{-1} \text{ yr}^{-1}$ at $z \approx 1$ and may be measured by optical telescopes using the Ly α forest or by radio telescopes using H I 21 cm or molecular absorption lines (Loeb 1998; Darling 2012). Proper motions of extragalactic objects may be caused by peculiar motions induced by large scale structure (Darling 2013; Darling & Truebenbach 2018; Truebenbach & Darling 2018), by primordial gravitational waves (e.g., Pyne et al. 1996; Gwinn et al. 1997; Book & Flanagan 2011; Darling et al. 2018), by the recession of fixed objects such as the baryon acoustic oscillation, or by anisotropic expansion (Fontanini et al. 2009; Quercellini et al. 2009; Titov 2009; Darling 2014).

Observer-induced proper motions are also possible: these include the secular aberration drift caused by acceleration of the solar system barycenter about the Galactic Center (e.g., Bastian 1995; Eubanks et al. 1995), observations from a rotating reference frame, and secular extragalactic parallax caused by motion with respect to the cosmic microwave background (CMB; Ding & Croft 2009).

Proper motions depict a discretely sampled vector field on the celestial sphere. In order to detect and characterize correlated motions, it is natural to describe vector fields using vector spherical harmonics (VSH), which are the vector equivalent of the scalar spherical harmonics used to describe signals such as the CMB temperature pattern, the geoid, or equipotentials (Mignard & Klioner 2012). VSH are characterized by their degree ℓ and order m , and resemble electromagnetic fields. They can therefore be separated into curl-free (E-mode) and divergenceless (B-mode) vector fields that are typically connected to distinct physical phenomena. The general method for characterizing a correlated proper motion field is to fit VSH to the observed proper motions and to calculate the power in and significance of each degree ℓ for each mode.

2. Expected (and Possible) Signals

Table 1 summarizes the expected and possible global extragalactic proper motion signals. This summary is likely to be incomplete. Here we provide a brief description of each physical or observer-induced effect, and Section 3 discusses the impact the ngVLA might have on detecting or constraining these phenomena.

2.1. Secular Aberration Drift

Aberration of light is caused by the finite speed of light and the motion of the observer with respect to a light source. The resulting deflection of light scales as \vec{v}/c . If the observer accelerates, then the aberration exhibits a secular drift, and objects appear to stream in the direction of the acceleration vector. The solar system barycenter accelerates at roughly $0.7 \text{ cm s}^{-1} \text{ yr}^{-1}$ as the Sun orbits the Galactic Center, resulting in an apparent $\sim 5 \mu\text{arcsec yr}^{-1}$ E-mode dipole converging on the Galactic Center (Figure 1). This has been detected in the proper motions of radio sources, first by Titov et al. (2011), using *a priori* knowledge of the expected effect for data trimming, and recently without priors by Truebenbach & Darling (2017). Titov & Krásná (2018) have further developed the VLBI-specific methodology for extracting this signal.

2.2. Secular Parallax

The CMB shows a temperature dipole of 3.4 mK, which is caused by the motion of the solar system barycenter with respect to the CMB rest frame (e.g., Hinshaw et al. 2009). This amounts to a relative motion of $369 \pm 0.9 \text{ km s}^{-1}$ or 78 AU yr^{-1} . This motion will induce a maximum secular parallax of $78 \mu\text{arcsec yr}^{-1} \text{ Mpc}^{-1}$: nearby galaxies in directions perpendicular to the CMB poles will show a reflex motion opposite our motion when compared to distant galaxies. Precise proper motion measurements of galaxies within $\sim 20 \text{ Mpc}$ will allow a statistical detection of the distance-dependent E-mode dipole caused by secular parallax. When referenced to this average dipole, it will be possible to detect the peculiar motions of individual galaxies as well as their geometric distances. Secular parallax may provide a distance ladder-free method for measuring distances in the local universe.

2.3. Rotation

As observers in a rotating reference frame, we have traditionally used quasars to define a fixed, non-rotating reference frame in order to measure and monitor the rotation of the Earth (e.g., McCarthy & Petit 2004). We thus have no means to detect non-terrestrial

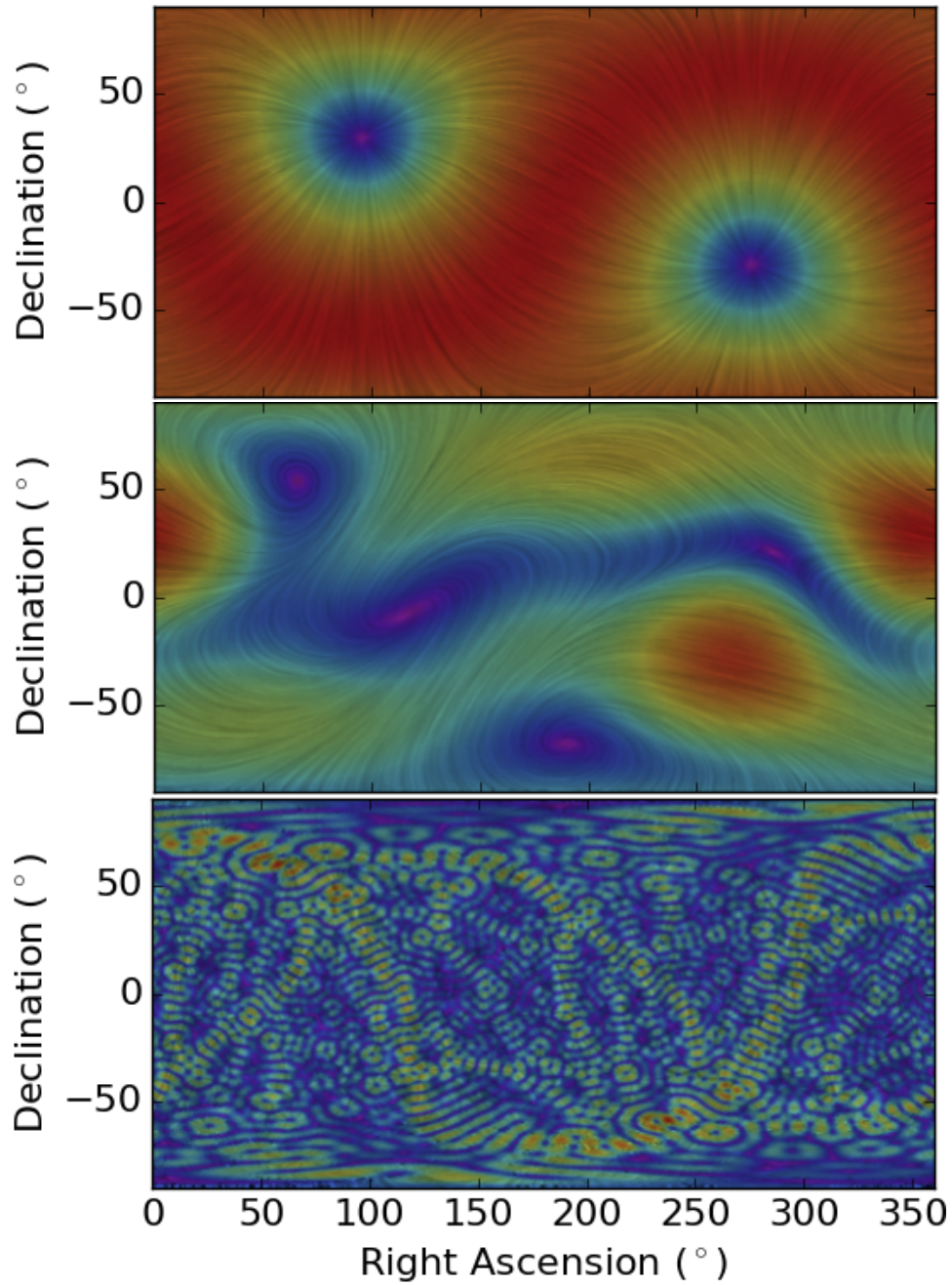


Figure 1. All-sky stream plots. Streamlines indicate the vector field direction, and the colors indicate the vector amplitude, from violet (zero) to red (maximum). Top: Secular aberration drift dipole detected by Truebenbach & Darling (2017). Middle: Randomly generated gravitational wave stream plot, after Darling et al. (2018). Bottom: Randomly generated BAO streamlines.

rotation that has an axis close to polar, but it is possible to detect or constrain rotation

about axes that are not aligned with the polar axis. While the question of a rotating universe can be nettlesome to contemplate and violates our assumption of cosmological isotropy, one can nonetheless make precise, sub- $\mu\text{arcsec yr}^{-1}$ measurements of the effect because it would manifest as a B-mode dipole in the proper motion vector field.

2.4. Anisotropic Expansion

In an isotropically expanding universe, objects move radially away from every observer (modulo small peculiar motions due to local density perturbations; see Section 2.6), so there will be no global correlated proper motions caused by isotropic Hubble expansion. However, anisotropic expansion would cause objects to stream across the sky toward the directions of fastest expansion and away from directions of slowest expansion. Assuming a simple triaxial anisotropy, one can show that the resulting celestial proper motion pattern can be completely described by an E-mode VSH quadrupole (Darling 2014). Fitting a curl-free quadrupole to a proper motion field can therefore measure or constrain the (an)isotropy of the Hubble expansion without *a priori* knowledge of H_0 . We can express the Hubble constant in terms of an angular rate, $H_0 \simeq 15 \mu\text{arcsec yr}^{-1}$, which means that a 10% anisotropy would produce a quadrupole with amplitude $1.5 \mu\text{arcsec yr}^{-1}$.

2.5. Gravitational Waves

Stochastic gravitational waves deflect light rays in a quadrupolar (and higher ℓ) pattern with equal power in the E- and B-modes (Figure 1; Pyne et al. 1996; Gwinn et al. 1997; Book & Flanagan 2011). The gravitational waves that will produce extragalactic proper motions lie in the frequency range $10^{-18} \text{ Hz} < f < 10^{-8} \text{ Hz}$ (H_0 to 0.3 yr^{-1}), which overlaps the pulsar timing and CMB polarization regimes, but uniquely covers about seven orders of magnitude of frequency space between the two methods (Darling et al. 2018). The cosmic energy density of gravitational waves Ω_{GW} can be related to the proper motion variance as

$$\Omega_{\text{GW}} \sim \langle \mu^2 \rangle / H_0^2 \quad (1)$$

and to the quadrupolar power P_2 as

$$\Omega_{\text{GW}} = \frac{6}{5} \frac{1}{4\pi} \frac{P_2}{H_0^2} = 0.00042 \frac{P_2}{(1 \mu\text{as yr}^{-1})^2} h_{70}^{-2} \quad (2)$$

(Gwinn et al. 1997; Book & Flanagan 2011; Darling et al. 2018). Measuring or constraining the proper motion quadrupole power can therefore detect or place limits on primordial gravitational waves in a unique portion of the gravitational wave spectrum.

2.6. Large Scale Structure

The mass density distribution of large-scale structure reflects the mass power spectrum, the shape and evolution of which relies on cosmological parameters. The transverse peculiar motions of extragalactic objects can be used to measure the density perturbations from large-scale structure without a reliance on precise distance measurements. While line-of-sight velocity studies use distances to differentiate Hubble expansion from peculiar velocity, peculiar motions across the line-of-sight are separable from Hubble expansion because no proper motion will occur in a homogeneous expansion (Nusser et al. 2012; Darling 2013). Thus, one can employ pairs of galaxies as “cosmic rulers”

to measure the real-time change in the apparent size of the rulers caused by the cosmic expansion and to detect structures that have decoupled from the Hubble flow (Darling 2013).

Given the definition of angular diameter distance, $\theta = \ell/D_A$, where a “ruler” of proper length ℓ subtends small angle θ at angular diameter distance D_A , cosmic expansion and a changing ℓ can produce an observed fractional rate of change in θ :

$$\frac{\Delta\theta/\Delta t_o}{\sin\theta} \equiv \frac{\dot{\theta}}{\sin\theta} = \frac{-\dot{D}_A}{D_A} + \frac{\dot{\ell}}{\ell} = \frac{-H(z)}{1+z} + \frac{\dot{\ell}}{\ell} \quad (3)$$

where $H(z) = H_o \sqrt{\Omega_{M,o}(1+z)^3 + \Omega_\Lambda}$ in a flat universe, Δt_o is the observer’s time increment, $\dot{\theta}$ is the *relative* proper motion, and $\dot{\ell}$ is the observed change in proper length, $\Delta\ell/\Delta t_o$, related to the physical (rest-frame) transverse velocity as $v_\perp = \dot{\ell}(1+z)$.

If ℓ is not a gravitationally influenced structure and grows with the expansion, then $\dot{\ell}/\ell = H(z)/1+z$, exactly canceling the first term in Eqn. (3). In this case, $\dot{\theta} = 0$, and there is no proper motion for objects co-moving with an isotropically expanding universe, as expected. If ℓ is decoupled from the expansion, however, then for most reasonable gravitational motions, $\dot{\ell}/\ell$ is a minor modification to the expansion contribution to $\dot{\theta}/\theta$ because the expansion, except for small redshifts or small structures, dominates (Darling 2013). The deviation of $\dot{\theta}/\theta$ from the null signal of pure Hubble expansion can be used to probe the mass distribution of large-scale structure and, thus, to test the shape of the mass power spectrum without a dependence on precise distance measurements or a “distance ladder.”

2.7. Baryon Acoustic Oscillation Evolution

The baryon acoustic oscillation (BAO) is a standard ruler arising from pre-CMB density fluctuations, which can be observed as an overdensity of galaxies on the scale of ~ 150 comoving Mpc (Eisenstein et al. 2005). At redshift $z = 0.5$, the BAO scale subtends $\theta_{BAO} = 4.5^\circ$, which is equivalent to VSH degree $\ell \sim 40$. Taking the time derivative, we obtain an expression for proper motion on these scales:

$$\mu_{BAO} = \frac{\Delta\theta_{BAO}}{\Delta t_o} \simeq -\theta_{BAO} H_o \simeq -1.2 \mu\text{as yr}^{-1}. \quad (4)$$

The BAO evolution will therefore manifest as a convergent E-mode signal around $\ell \sim 40$ (Figure 1). To first order, the BAO scale depends on the expansion rate $H(z)$ and the angular diameter distance $D_A(z)$ at the observed redshift, but the rate of change of this standard ruler is dominated by its recession (“receding objects appear to shrink”) and depends to first order on $H_o/D_A(z)$. Detection of this effect relies critically on the sky density of sources, which must adequately sample angular scales smaller than 4.5° .

3. ngVLA Science

The ngVLA can detect or constrain all of these phenomena and improve upon many of the expected *Gaia* measurements. Table 1 lists the various proper motion signals, their VSH modes, the expected amplitude of the signal (if known), a recent measurement (if any), and predictions for *Gaia* and the ngVLA. We make the following assumptions about a ngVLA astrometry program:

Table 1. Global Correlated Proper Motion Signals

Effect	ℓ	Mode	Amplitude ($\mu\text{arcsec yr}^{-1}$)	Recent Measurement ($\mu\text{arcsec yr}^{-1}$)	Ref	<i>Gaia</i> (Predicted)	ngVLA (Predicted)	Prev. Work
Secular Aberration Drift	1	E	~ 5	5.2 ± 0.2	1	10σ	50σ	2,3,4,5
Secular Parallax	1	E	78 Mpc^{-1}	$\sim 10\sigma$	$\sim 10\sigma^{(1)}$	6
Rotation	1	B	Unknown	0.45 ± 0.27	7	$< 0.5 \mu\text{as yr}^{-1}$	$< 0.1 \mu\text{as yr}^{-1 (2)}$	2,5,7
Anisotropic Expansion	2	E	Unknown	$< 7\%$	8	$< 3\%$	$< 0.7\%$	8,9,10,11
Gravitational Waves	≥ 2	E+B	Unknown	$\Omega_{GW} < 6.4 \times 10^{-3}$	7	$\Omega_{GW} < 4 \times 10^{-4}$	$\Omega_{GW} < 10^{-5}$	1,7,12,13,14,15,16
Large Scale Structure	$\gtrsim 5$	E	$-1.5 \text{ to } +5$	8.3 ± 14.9	17	10σ	$\sim 20\sigma^{(3)}$	17,18,19
BAO Evolution	~ 40	E	$-1.2 \text{ at } z = 0.5$	4σ	$\sim 10\sigma^{(4)}$...

Notes: 1 – Detection of the secular parallax is limited by the number of compact radio sources that can (and would) be monitored in the local volume. 2 – ngVLA observations will only be sensitive to rotation axes that are not aligned with the Earth’s rotation axis. 3 – Detection of peculiar velocities associated with large scale structure will depend on the number of close pairs of radio sources. 4 – Detection of the BAO evolution signal will depend strongly on the sky density of proper motion measurements.
 References: 1 – Tiouv & Krásná (2018) 2 - Tiouv et al. (2011); 3 – Xu et al. (2012); 4 – Tiouv & Lambert (2013); 5 – Truebenbach & Darling (2017); 6 – Ding & Croft (2009); 7 – Darling et al. (2018); 8 – Darling (2014); 9 – Chang & Lin (2015); 10 – Bengaly (2016); 11 – Paine et al. (2018); 12 – Braginsky et al. (1990); 13 – Pyne et al. (1996); 14 – Kaiser & Jaffe (1997); 15 – Gwinn et al. (1997); 16 – Book & Flanagan (2011); 17 – Darling (2013); 18 – Darling & Truebenbach (2018); 19 – Truebenbach & Darling (2018).

- A sample of 10,000 objects
- Astrometric observations spanning 10 years
- VLBA-level astrometric precision: $\pm 10 \mu\text{as yr}^{-1}$ per object

Implicit in these assumptions are VLBA-sized baselines with roughly ten times the current VLBA collecting area. We further assume that radio jets will pose the same challenges as are found in the current VLBA data. In practice, we simply scale current VLBA-based observations — which include the added intrinsic proper motion “noise” contribution from relativistic jets — by N or \sqrt{N} , as appropriate, to the expected ngVLA sample. The proposed sample is roughly ten times larger than current VLBA geodetic monitoring samples, but an increased collecting area would enable the ngVLA (or a long-baseline subarray) to monitor the expanded sample without increasing the observing time commitment. The ngVLA sample would leverage the current VLBA sample and the radio-loud *Gaia* AGN, providing super-decade time baselines for a significant subset of objects.

The proposed observations will enable global detection of correlated signals of $\sim 0.1 \mu\text{as yr}^{-1}$, which is $\sim 0.7\%$ of H_0 . For most of the phenomena described in Section 2, the ngVLA would significantly improve on previous work, including the expected *Gaia* performance. While the ngVLA sample size will be a factor of ~ 50 smaller than the *Gaia* sample, the per-source astrometry will be a factor of ~ 20 – 50 times better. We therefore predict that ngVLA observations will substantially improve on *Gaia* global correlated proper motion measurements in most cases. The proposed ngVLA program may not perform as well as our expectations for *Gaia* for measurements requiring fine angular sampling (BAO evolution) or dense volumetric sampling (secular parallax). This is due to the overall physical paucity of compact radio sources compared to optical sources across the sky and in the very nearby universe.

4. Conclusions

The outlook for extragalactic proper motions using the ngVLA is promising, and in most cases it can surpass the expected performance of *Gaia*, despite the added challenge of the intrinsic proper motion caused by radio jets. In particular, the proposed ngVLA astrometry program would provide exquisite precision on the Solar motion in the Galaxy and place the strongest constraints to date on the isotropy of the Hubble expansion in the epoch of dark energy and on the primordial gravitational wave background over roughly 10 decades in frequency.

Acknowledgments. The authors acknowledge support from the NSF grant AST-1411605 and the NASA grant 14-ATP14-0086.

References

- Bastian, U. 1995, in ESA Special Publication, Vol. 379, Future Possibilities for Astrometry in Space, ed. M. A. C. Perryman & F. van Leeuwen, 99
- Bengaly, C. A. P., Jr. 2016, JCAP, 4, 036
- Book, L. G. & Flanagan, É. É. 2011, Phys. Rev. D, 83, 024024
- Bower, G. C., Demorest, P., Braatz, J., et al. 2015, ArXiv e-prints, arXiv:1510.06432
- Braginsky, V. B., Kardashev, N. S., Polnarev, A. G., & Novikov, I. D. 1990, Nuovo Cimento B, 105, 1141

- Chang, Z., & Lin, H.-N. 2015, MNRAS, 446, 2952
Darling, J. 2012, ApJ, 761, L26
Darling, J. 2013, ApJ, 777, L21
Darling, J. 2014, MNRAS, 442, L66
Darling, J. & Truebenbach, A. E. 2018, ApJ, 864, 37
Darling, J., Truebenbach, A., & Paine, J. 2018, ApJ, 861, 113
Ding, F., & Croft, R. A. C. 2009, MNRAS, 397, 1739
Eisenstein, D. J., Zehavi, I., David W. Hogg, D. W., et al. 2005, ApJ, 633, 560
Eubanks, T. M., Matsakis, D. N., Josties, F. J., et al. 1995, in IAU Symposium, Vol. 166, Astronomical and Astrophysical Objectives of Sub-Milliarcsecond Optical Astrometry, ed. E. Hog & P. K. Seidelmann, 283
Fontanini, M., West, E. J., & Trodden, M. 2009, Phys. Rev. D, 80, 123515
Gwinn, C. R., Eubanks, T. M., Pyne, T., Birkinshaw, M., & Matsakis, D. N. 1997, ApJ, 485, 87
Hinshaw, G., Weiland, J.L., Hill, R.S., et al. 2009, ApJS, 180, 225
Kaiser, N. & Jaffe, A. 1997, ApJ, 484, 545
Loeb, A. 1998, ApJ, 499, L111
McCarthy, D. D., & Petit, G. 2004, IERS Technical Note, 32
Mignard, F. & Klioner, S. 2012, A&A, 547, A59
Nusser, A., Branchini, E., & Davis, M. 2012, ApJ, 755, 58
Paine, J., Darling, J., & Truebenbach, A. 2018, ApJS, 236, 37
Pyne, T., Gwinn, C. R., Birkinshaw, M., Eubanks, T. M., & Matsakis, D. N. 1996, ApJ, 465, 566
Quercellini, C., Quartin, M., & Amendola, L. 2009, Phys.Rev.Lett, 102, 151302
Sandage, A. 1962, ApJ, 136, 319
Titov, O. 2009, in Proc. 19th European VLBI for Geodesy and Astrometry (EVGA) Working Meeting, ed. G. Bourda, et al., 14
Titov, O., Lambert, S. B., & Gontier, A.-M. 2011, A&A, 529, A91
Titov, O., & Lambert, S. 2013, A&A, 559, A95
Titov, O., & Krásná, H. 2018, A&A, in press
Truebenbach, A. E., & Darling, J. 2017, ApJS, 233, 3
Truebenbach, A. E., & Darling, J. 2018, ApJ, in press (arXiv:1808.07103)
Xu, M. H., Wang, G. L., & Zhao, M. 2012, A&A, 544, A135